Part II

Plasma-Assisted Nitrogen Fixation

3

Introduction to Plasma Technology

Anthony B. Murphy

CSIRO, Manufacturing, Lindfield, NSW, Australia

3.1 Fundamental Concepts

Plasmas are often described as the fourth state of matter; as energy is added, a substance is transformed from a solid to a liquid, then to a gas, and finally to a plasma. The transformation that occurs when a plasma is formed is that some of the gas molecules are ionized to form ions and electrons. Hence, the term "ionized gas" is often used to describe a plasma. The term "plasma" was first introduced by Langmuir [1] to describe the regions in an ionized gas in which the electron and ion charges were balanced. Plasmas are generally composed of a range of species, including molecules, radicals, atoms, molecular and atomic ions (collectively termed the heavy species or heavy particles), electrons, and photons.

3.1.1 Types of Plasma

Most of the visible matter in the universe (at least 99.9%) is in the plasma state. Stars and the interstellar medium are composed of plasma, as is the Earth's ionosphere. On Earth, plasmas are much less common, but lightning arcs, sparks, flames, and the polar aurora are all examples of naturally occurring plasmas. As will be discussed in Section 3.4, plasmas are also of immense practical importance, so a wide range of man-made plasmas are routinely produced and applied.

These examples indicate that plasmas exist across a wide range of parameters. Plasmas can be classified according to their properties, including the pressure, the electron density, the degree of ionization, and the temperature. Several different temperatures can be defined, as will be discussed below; the most important is

Plasma-Assisted Nitrogen Fixation for Sustainable Process Industries, First Edition. Edited by Volker Hessel, Annemie Bogaerts, Gabriele Centi, Evgeny Rebrov, and Nguyen Van Duc Long.

Published 2026 by John Wiley & Sons, Inc.

the electron temperature, which describes the translational temperature of the electrons. There is a strong interdependence of the different properties; e.g. the electron density depends on the pressure and the degree of ionization, which in turn depends on the electron and possible other temperatures.

A widely used classification, shown in Figure 3.1, considers the electron density n_e and the electron temperature T_e. The range of electron densities varies from around 10^8 to 10^{24} m^{-3} and depends on the pressure and the degree of ionization. Pressures range from high vacuum to above atmospheric, and the degree of ionization ranges from very low (as low as 10^{-10} in flames) to full or multiple ionization in thermal and thermonuclear fusion plasmas.

Of the man-made plasmas, thermonuclear fusion plasmas have high electron temperatures and densities, like those in the solar core, which is consistent with the goal of thermonuclear fusion research – to drive nuclear fusion reactions like those occurring in the sun.

Plasmas of industrial interest – glow discharges, non-equilibrium atmospheric pressure discharges such as dielectric barrier discharges (DBDs), warm plasmas such as microwave and spark discharges, and thermal arc and RF discharges – have approximately similar electron temperatures, typically in the range of 1–20 eV (1 eV $\sim$ 11,600 K), but span a range of electron densities. The characteristics of such plasmas will be discussed in Section 3.4.

3.1.2 Scaling Parameters

While a conventional description of a plasma is as an ionized gas, most definitions are more restrictive. Typical definitions require quasineutrality, i.e. that the negatively and positively charged particles balance each other. Quasineutrality is driven by the electric field that is formed due to any separation between the electrons and ions, which counteracts their separation. Deviations from quasineutrality can occur within a characteristic length scale known as the Debye length, which describes the smallest length scale of a plasma, given by

$$\lambda_{\mathrm{D}} = \left(\frac{\varepsilon_0 k_B T_e}{n_e e^2} \right)^{1/2} \tag{3.1}$$

where ε_0 is the permittivity of free space, e is the electronic charge, and k_B is Boltzmann's constant. The dependence of Debye length on electron temperature and electron density is shown in Figure 3.2a. Deviations from quasineutrality occur in the sheath regions at the boundary between electrodes and the plasma, whose thickness is typically several λ_{D}, and within the heads of streamers, which are discussed in Section 3.2. Another requirement for a plasma is that at least several electrons are present within a sphere of radius λ_{D}; i.e.

$$\frac{4}{3}\pi n_e \lambda_{\mathrm{D}}^3 > 1 \tag{3.2}$$

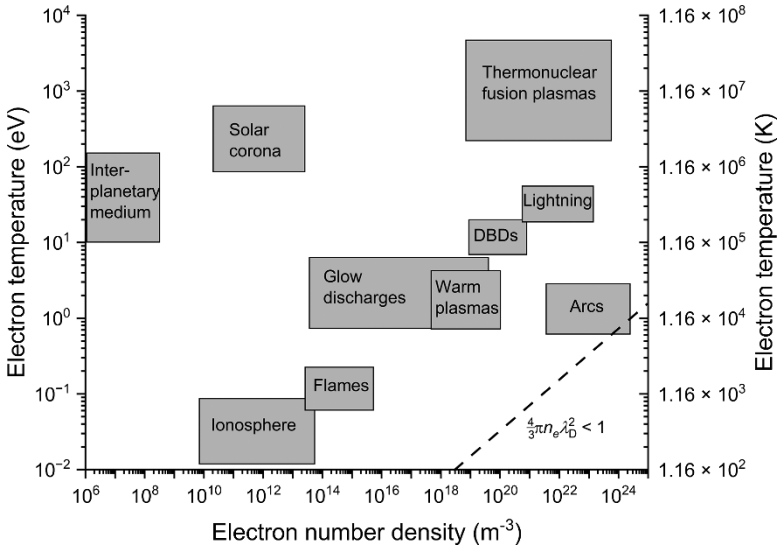

Figure 3.1 Plasmas classified by electron temperature and electron density.

The range of electron temperatures and densities over which this criterion applies is indicated in Figure 3.1.

Two important frequencies are the electron and ion plasma frequencies, given by

$$\omega_{pj} = \left(\frac{n_j Z_j^2 e^2}{\varepsilon_0 m_j}\right)^{1/2} \tag{3.3}$$

where n_j is the number density, Z_j is the charge number, and m_j is the mass of species j, which can be the electron or an ion. The plasma frequency determines whether a species can follow an applied electric field; if the frequency of the applied field is higher than ω_{pj}, then species j cannot follow the field. The dependence of ω_{pj} on electron density is shown for electrons and atomic hydrogen and argon ions in Figure 3.2b.

The concept of temperature is more complex for a plasma than a non-ionized gas. Many processes contribute to the energy of the plasma, including the translational energy of each species, the rotational and vibrational excitation of molecules and molecular ions, and the electronic excitation of molecules, atoms, and ions. Each of these can be described by a distribution function and temperature, with thermal equilibrium of a given species leading to the Maxwell–Boltzmann distribution:

$$f(\boldsymbol{v}_j) = \left(\frac{m_j}{2\pi k_B T_j}\right)^{3/2} \exp\left(\frac{\frac{1}{2} m_j v_j^2}{k_B T_j}\right) \tag{3.4}$$

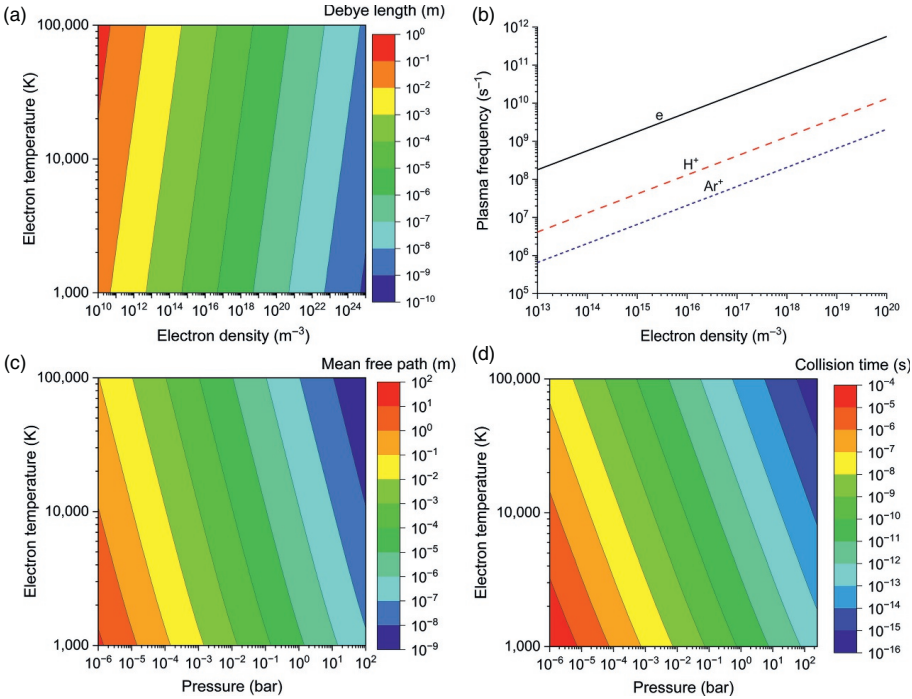

Figure 3.2 (a) Debye length; (b) electron, hydrogen ion, and argon ion plasma frequency; (c) mean free path; (d) mean time between collisions (c) and (d) are for electrons in a weakly ionized argon plasma with heavy particle temperature of 300 K.

where $\boldsymbol{v}_j$, m_j, and T_j are the velocity, mass, and temperature of the jth species. The mean energy is given by $3k_BT_j/2$, and the average velocity is

$$\overline{v_j} = \left(\frac{8k_BT_j}{\pi m_j}\right)^{1/2} \tag{3.5}$$

The average kinetic energy exchange during an elastic binary condition between particles of mass m_j and m_k is given by [2]:

$$\Delta E_{\text{kin}} = \frac{2m_jm_k}{\left(m_j + m_k\right)^2}\left|E_{\text{kin}\,j} - E_{\text{kin}\,k}\right| \tag{3.6}$$

where $\left|E_{\text{kin}\,j} - E_{\text{kin}\,k}\right|$ is the difference in kinetic energy of the particles. For particles of the same mass, $\Delta E_{\text{kin}} = 1/2\left|E_{\text{kin}\,j} - E_{\text{kin}\,k}\right|$, and only around 10 successive collisions are required to eliminate distortions in the Maxwell–Boltzmann distribution. However, particularly at low pressures for which the time between collisions is relatively large, deviations from the Maxwell–Boltzmann distribution can occur, e.g. due to fluxes of energetic species from the wall (e.g. electrons released by ion impact) [3].

For the case of a collision between an electron and a heavy particle of masses m_e and m_h, respectively, Eq. (3.6) gives $\Delta E_{\text{kin}} = 2(m_e/m_h)\left|E_{\text{kin}\,j} - E_{\text{kin}\,k}\right|$. Since $m_e \ll m_h$, a large number of collisions, at least 10,000, are required to equilibrate the temperatures of electrons and heavy species.

Energy is usually supplied to a plasma through an electric or electromagnetic field. While collisions act to equilibrate the species temperatures, the field accelerates the electrons, with the electron energy acquired between collisions given by

$$\Delta E_{\text{kin}\,e} = eE\overline{v_{de}}\,\overline{\tau_e} \tag{3.7}$$

where E is the electric field strength and $\overline{v_{de}}$ is the mean electron drift velocity. The drift velocity is given by

$$\overline{v_{de}} = \frac{\overline{\tau_e}}{m_e}eE \tag{3.8}$$

where $\overline{\tau_e} = \overline{l_e}/\overline{v_{de}}$ is the mean time between electron collisions with $\overline{l_e}$ denoting the electron mean free path. For a plasma that is weakly ionized ($n_e/n \ll 1$, n being the total or gas number density), the mean free path is given by

$$\overline{l_e} = 1/(nQ_{ea}) \tag{3.9}$$

where the momentum transfer cross-section for electron–atom collisions is $Q_{ea} \approx (3.6 \times 10^{-4}T_e - 0.1) \times 10^{-20}\ \text{m}^2$ for an argon plasma [4, 5]. The value of Q_{ea} depends on the type of plasma. Its dependence on the electron temperature and pressure for argon is given in Figure 3.2c. Data for different plasmas can be found in Refs. [6, 7].

Equating $\Delta E_{\text{kin}\,e}$ with the energy exchange in a collision between an electron and heavy species,

$$\Delta E_{\text{kin}\,e} = (2m_e/m_h)3k_B(T_e - T_h)/2 \tag{3.10}$$

gives an estimate for the relative temperature difference [8].

$$\frac{T_e - T_h}{T_e} = \frac{3\pi}{32}\frac{m_h}{m_e}\left(\frac{e\overline{l_e}E}{\frac{3}{2}k_B T_e}\right)^2 \tag{3.11}$$

where T_h is the heavy-particle temperature. The inverse dependence of $\overline{l_e}$ on n (Eq. (3.9)) indicates that the ratio E/n, known as the reduced electric field, plays an important role in determining the kinetic equilibrium between electrons and heavy particles.

Figure 3.2d shows the dependence of $\overline{\tau_e}$ on the pressure and the electron temperature for a heavy-particle temperature T_h of 300 K in a weakly ionized argon plasma. $\overline{\tau_e}$ is inversely proportional to T_h, so results for higher heavy-particle temperatures are easily determined from the figure.

For an atmospheric-pressure plasma with $T_e = 10{,}000$ K and $T_h = 300$ K, $\overline{\tau_e} \approx 1.7$ ps, indicating that equilibration between electrons and heavy particles will require at least tens to hundreds of nanoseconds. At low pressures, $\overline{\tau_e}$ is much larger.

A further scaling parameter, relevant to high-frequency excitation of the plasma, is $\omega\overline{\tau_e}$, where ω is the angular frequency of the applied voltage. Power transfer from the electric field is maximized for $\omega\overline{\tau_e} \approx 1$. This is achievable at low pressures using RF and microwave sources, since, as shown in Figure 3.2d, $\overline{\tau_e}$ is in the micro- to nanosecond range. However, at atmospheric pressure, the picosecond values of $\overline{\tau_e}$ would require excitation in the terahertz range, indicating that the power transfer is far from optimal, even for microwave sources.

3.2 Plasma Generation

Plasmas are generated by electrical breakdown – the formation of electrons and ions under the influence of an electric field. Breakdown occurs when the production of these charged species (i.e. ionization) overcomes their tendency to recombine to form neutral molecules or attach to molecules to form negative ions (i.e. recombination). Figure 3.3 summarizes the transitions that can occur that lead to the formation of different types of discharges.

A low density of seed electrons, of order 10^9–10^{10} m^{-3}, is always present in a gas because of the action of cosmic rays and background radioactivity [10]. An electric field accelerates these electrons, which can then attain the energy required to

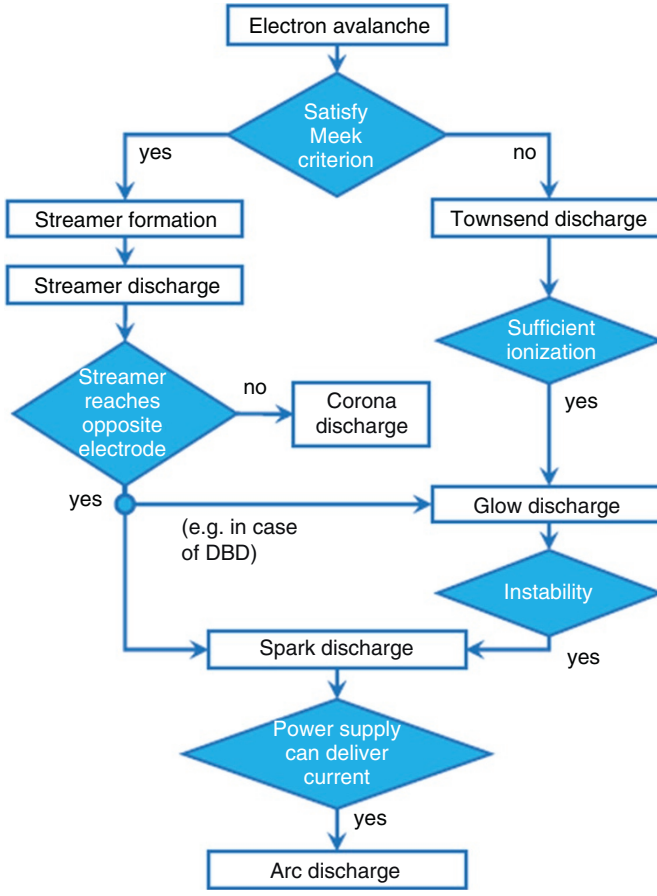

Figure 3.3 Summary of the transitions that can occur in the formation of discharges. *Source:* Reproduced from Ref. [9]/with permission of IOP Publishing.

ionize surrounding molecules. This leads to exponential growth of the electron density, forming an avalanche. The ionization coefficient (also known as the first Townsend coefficient), which gives the number of electrons produced per unit length, can be approximated as [3, 11].

$$\alpha = Ap \exp(-Bp/E) \tag{3.12}$$

where A and B are constants that depend on the gas. Recombination is described by a second Townsend coefficient β, and a third Townsend coefficient γ describes the production of electrons by the impact of ions on surfaces.

In a DC field between two electrodes separated by a distance d, electrons drift toward the anode (the positive electrode) and are lost upon reaching it. Maintaining the discharge (known as a Townsend discharge) requires enough secondary electrons to be produced by the interaction of the ions with the cathode (the negative electrode). The Paschen criterion for breakdown requires that sufficient ions are produced by ionization for the secondary electrons produced at the cathode to replace those lost at the anode. It provides a relation between the breakdown voltage V_b and the product pd [3, 11].

$$V_b = B(pd)/[C + \ln(pd)] \tag{3.13}$$

where

$$C = \ln \frac{A}{\ln(1/\gamma) + 1} \tag{3.14}$$

The function $V_b(pd)$ has a minimum value at

$$(pd)_{\min} = (e/A)[\ln(1/\gamma) + 1] \tag{3.15}$$

At lower values of pd, the electron avalanche reaches the anode before sufficient ions have been produced, requiring a higher electric field (and, therefore, voltage) to increase ionization. At higher values of pd, the number of collisions increases, and the electric field decreases for a given voltage, so the voltage again must be increased.

For high-frequency electric fields, the breakdown mechanism is different because the electron avalanche develops as time progresses but does not reach the anode because of the rapid change in polarity. In this case, breakdown requires that the energy gain of electrons from the electric field balance losses by collisions with the neutral gas, averaged over time [3].

With increasing pressure, the mean free path $\overline{l_e}$ (Eq. (3.9)) decreases because of the increased number density n. At atmospheric pressure, its value is around 10 μm, much less than the distance between electrodes, so the influence of secondary electrons vanishes. At high pressure, breakdown proceeds by the formation of streamers. A streamer head containing a high charge density is formed, generating a high electric field, which causes further ionization, leading to the propagation of the streamer head toward the electrode of opposite polarity. The propagation mechanism depends on the polarity of the electrode toward which the streamer is propagating [9]. The streamer head is trailed by a streamer channel, which is slowly neutralized by recombination.

Two main criteria have been found in the literature for the transition of an electron avalanche to a streamer [12]. The first is that the background field must be high enough for electron-impact ionization to dominate recombination reactions. In dry air, the primary recombination mechanism is the attachment of electrons to molecules to form negative ions. Figure 3.4 shows that the ionization

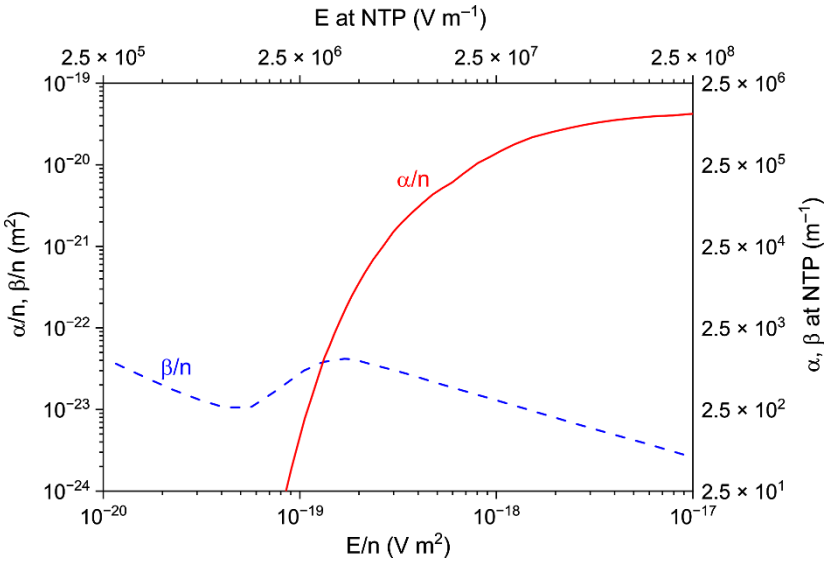

Figure 3.4 Values of the ionization and recombination coefficients as a function of the electric field, all normalized to the gas density for dry air. Unnormalized values at NTP (normal temperature and pressure, 293.15 K and 1 atm) are also shown. *Source:* Adapted from [13].

coefficient α increases rapidly with the E/n, as per Eq. (3.12), while the recombination coefficient β has a relatively weak dependence on E/n. Initial breakdown requires about 2 MV m^{-1} at 1 bar. Once breakdown has occurred, this is reduced to about 0.5 MV m^{-1} due to the presence of excited molecules, which can detach electrons from negative ions [13]. The second criterion to be satisfied is known as the Meek or Raether–Meek condition and requires that the number of electrons must reach 10^8–10^9 for significant space charge effects to occur (i.e. for the charge to modify the electric field); if this occurs by exponential multiplication of an initial electron in the background electric field, it requires

$$\exp[(\alpha-\beta)d_{\text{ion}}] \approx 10^8 \text{ to } 10^9 \tag{3.16}$$

i.e. $\alpha d_{\text{ion}} \approx 18$ to 21, where d_{ion} is the ionization length of the local avalanche (for which $\alpha - \beta > 0$). The Meek condition is an approximate criterion and has been modified to take into account many other factors (e.g. Ref. [12]).

A corona discharge occurs when αd_{ion} is at least around 9 [14] but does not meet the Meek condition and does not cross the full distance to the other electrode. If, however, the streamer crosses the full distance between the electrodes, a conductive channel is formed. Gas heating occurs through collisions on a time scale of

~100 ns at 1 bar, as discussed in Section 3.1.2, and a spark is produced. This can progress to an arc discharge on a time scale of ~100 μs if the power supply can deliver the required current (in the range of amperes to kiloamperes or more) [9]. If, however, the time scale of the discharge is limited to substantially less than required for gas heating, e.g. by the introduction of a dielectric barrier between the electrodes, as in a DBD, or by removing the voltage, as in a nanosecond-pulsed power supply, a glow discharge is produced.

3.3 Plasma Chemistry

The presence of energetic electrons and the species that they produce provides access to a much wider range of chemical reactions in plasmas than occurs in a non-ionized gas. As discussed in Section 3.1.2, the electrons are accelerated in the electric field and transfer energy to heavy particles through collisions. In that section, elastic collisions, in which kinetic energy is conserved, were considered. Inelastic collisions, in which kinetic energy is not conserved, also occur; in such cases, the composition or internal energy of at least one of the particles involved in the collision is changed. The collision partners can be an electron and a heavy particle or a pair of heavy particles; three-body collisions can also be important. Plasma chemistry is mainly driven by these inelastic collisions. Chemistry can also be driven by photons (e.g. photoionization is important in the propagation of streamers propagating toward the cathode) and by reactions occurring on surfaces.

3.3.1 Inelastic Collisions Between Electrons and Heavy Particles

Inelastic collisions with electrons can transfer the kinetic energy of electrons into the internal energy of atoms and molecules via rotational, vibrational, and electronic excitation of molecules and electronic excitation of atoms. Further, inelastic collisions can cause dissociation of molecules and ionization of atoms and molecules. Superelastic collisions, in which the internal energy of excited molecules or atoms is transferred back into the kinetic energy of electrons, can also occur.

The reactions depend strongly on the energy of the electrons, which in turn depends on the reduced electric field E/n. The mean electron energy for a Maxwell–Boltzmann distribution of electron energies (Eq. (3.4)) is $(3/2)k_B T_e$. The distribution has a high-energy tail so that reactions requiring well over the mean electron energy can occur.

Electron-impact vibrational excitation of molecules is an important process in non-equilibrium atmospheric-pressure plasmas. As shown in Figure 3.5, it dominates the energy transfer from electrons to molecules at low electron energies, up to a few eV. While the optimum electron energy range and the cross-section

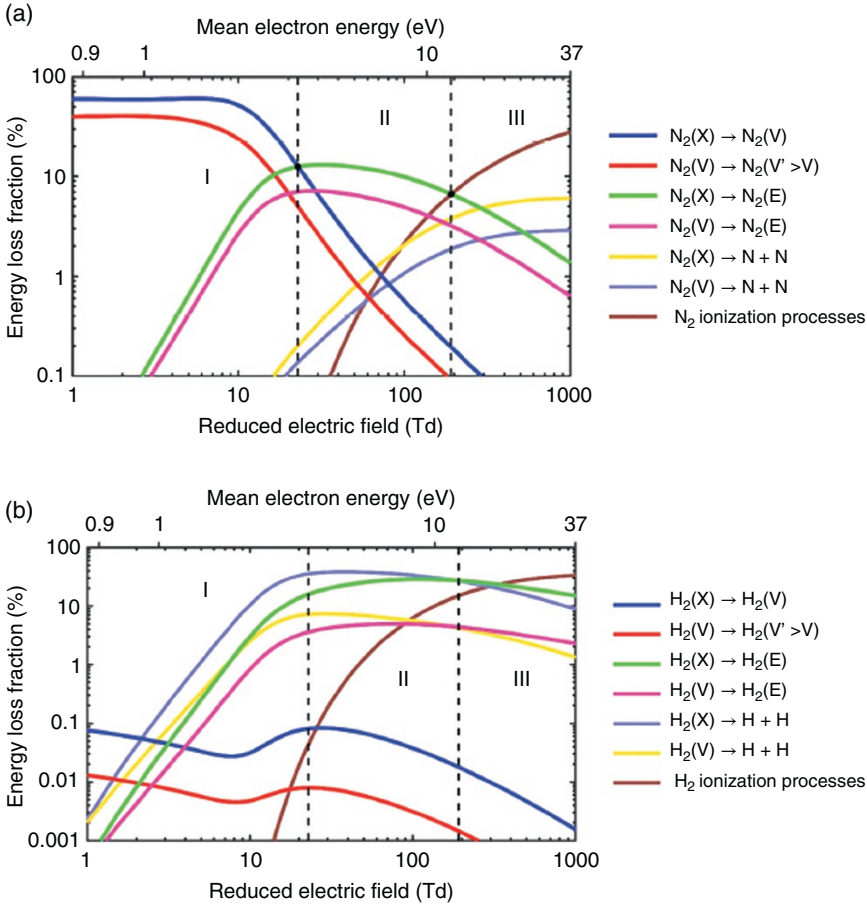

Figure 3.5 Fraction of electron energy transferred to (a) nitrogen and (b) hydrogen species in a 3:1 mixture of N_2 and H_2 with T_g = 400 K and T_{vib} = 300 K. (X), (V), and (E) denote ground state, vibrationally excited, and electronically excited levels, respectively. 1 Td = 10^{-21} V m^2. *Source:* Ref. [15]/Royal Society of Chemistry/CC BY 3.0.

depend on the gas, vibrational excitation is typically most effective in the range $T_e \sim 1$–3 eV, with almost every electron–molecule collision leading to vibrational excitation at 2 eV for N_2, CO_2, and CO [16]. As shown in the figure, the electron energy is related to the reduced electric field E/n, which is often given in units of townsend; 1 Td = 10^{-21} V m^2. At 1 bar, 1 Td corresponds to an electric field of 2.5×10^4 V m^{-1}.

Rotational excitation requires far less energy than vibrational excitation and typically proceeds by "quasi-elastic" energy transfer, with each collision transferring

m_e/m_h of the electron energy. This typically ensures that the rotational temperature $T_{\text{rot}} \approx T_h$ at or near 1 bar.

Electronic excitation of atoms and molecules requires higher electron energies, usually of the order of 5 eV or more, as shown in Figure 3.5. For example, the first excited level ($A\ ^3\Sigma_{u+}$) of a nitrogen molecule is about 8.0 eV, and the first excited level of an argon atom is 11.55 eV.

Dissociation through electronic excitation can be caused by a single collision via several mechanisms; those requiring the lowest energy are excitation to a repulsive molecular state and excitation to an attractive state with energy exceeding the dissociation threshold. As shown in Figure 3.5, dissociation requires high electron energies, particularly in the case of strong bonds such as the nitrogen triple bond.

Ionization can occur directly from the ground state of an atom or molecule through a collision with a sufficiently energetic electron. The first ionization energies of an argon atom, a nitrogen atom, and a nitrogen molecule are 15.8, 14.5, and 15.6 eV, respectively. Stepwise ionization, i.e. ionization of an excited atom or molecule, can also occur. Direct ionization is favored by high electron energies (see Figure 3.5) and low concentrations of excited species.

In addition to the above endothermic reactions, electron interactions with energetic species, such as electron–ion recombination, can release significant energy. In a molecular gas, electron–ion recombination can lead to dissociation (dissociative electron–ion recombination – $e + \mathbf{AB}^+ \rightarrow \mathbf{AB}^* \rightarrow \mathbf{A} + \mathbf{B}^*$). In atomic gases, three-body electron–ion recombination ($e + e + \mathrm{A}^+ \rightarrow \mathrm{A}^* + e$), with the excess energy being transferred to an electron, is important. Radiative electron–ion recombination ($e + \mathrm{A}^+ \rightarrow \mathrm{A}^* \rightarrow \mathrm{A} + h\nu$), in which the excess energy is converted into radiation, can also be important when the electron density is low.

A range of reactions that form negative ions can also occur. In non-equilibrium atmospheric-pressure discharges, three-body electron attachment ($e + \mathbf{A} + \mathbf{B} \rightarrow \mathbf{A}^- + \mathbf{B}$) can be important, e.g. in the formation of O_2^- ions. At lower pressures, when three-body reactions are less likely, dissociative electron attachment ($e + \mathbf{AB} \rightarrow (\mathbf{AB}^-)^* \rightarrow \mathbf{A} + \mathbf{B}^-$) can be important; the cross-section depends strongly on the electron energy and has a peak at relatively high energies, around 6 eV for O_2 and 10 eV for CO, except for halogen molecules [16]. Electron impact detachment ($e + \mathbf{A}^- \rightarrow \mathbf{A} + e + e$) is an important detachment mechanism for high degrees of ionization; associative detachment (see Section 3.3.2) dominates in non-equilibrium discharges.

3.3.2 Inelastic Collisions Between Heavy Particles

Collisions between pairs of ground-state atoms or molecules are generally elastic. However, if one or more of the particles are excited, a wide range of inelastic collisions can occur. These include VT relaxation, in which energy is transferred from

vibrational excitation to translational kinetic energy; VV relaxation, in which vibrational energy is transferred from one vibrationally excited molecule to another; the analogous RT and RR relaxation processes that involve rotationally excited molecules; and relaxation of electronic excitation to vibrational and rotational excitation and translational kinetic energy.

VT relaxation is slow unless chemical reactions occur. This can lead to high levels of vibrational excitation in gases such as N_2, H_2, CO, and CO_2 for non-equilibrium discharges. VV collisions can lead to "ladder-climbing," with vibrational energy transferred from one excited molecule to another.

In contrast, RT collisions are relatively fast, and rotational and translational temperatures are generally similar in atmospheric-pressure plasmas, as noted in Section 3.3.1.

Relaxation of electronic excitation to translational energy is very slow, while transfer to vibrational energy can occur through formation of intermediate complexes and can be relatively fast. When the degree of ionization exceeds 10^{-6}, transfer of electronic energy is dominated by superelastic collisions with electrons [16].

Vibrational and electronic excitations increase the rate of endothermic reactions. The reaction rate coefficient in the case of vibrational excitation can be expressed as

$$k_R(E_{\text{vib}}, T_h) = k_{R0} \exp\left(-\frac{E_a - \alpha_{\text{FM}} E_{\text{vib}}}{k_B T_h}\right) \tag{3.17}$$

when the activation energy $E_a > \alpha_{\text{FM}} E_{\text{vib}}$, where k_{R0} is the pre-exponential term for ground-state molecules, E_{vib} is the vibrational excitation energy, and α_{FM} is the efficiency of the excitation energy in overcoming the reaction barrier. For exchange-type reactions $\mathbf{A} + \mathbf{BC} \rightarrow \mathbf{AB} + \mathbf{C}$, the Fridman–Macheret α-model gives an approximate expression:

$$\alpha_{\text{FM}} = E_{af} / \left(E_{af} + E_{ar}\right) \tag{3.18}$$

where f and r denote the forward and reverse reactions, respectively. The value of α_{FM} is close to 1 for strongly endothermic reactions with activation energy close to the reaction enthalpy and close to 0 for exothermic reactions without activation energy [16]. Electronic excitation is harder to analyze, but the same general trends apply.

Dissociation of molecules through heavy-particle collisions requires at least one of the molecules to be excited. In the absence of electronic excitation, dissociation is a multi-step process requiring collisions between vibrationally excited molecules to transfer enough energy to one of the molecules to dissociate; this process is effective for a limited group of gases that includes N_2, H_2, CO, and CO_2.

While electron-impact ionization requires an electron with kinetic energy only slightly more than the ionization potential, heavy-particle collisions transfer much less energy to bound electrons. Ionization requires the colliding heavy particle to have a kinetic energy of 10–100 keV, which is rare in plasmas of industrial interest. However, the internal energy of one or more of the heavy particles can promote ionization. Penning ionization occurs when a metastable atom with excitation energy E_m collides with another atom with ionization energy $E_{\text{ion}} < E_m$. This is particularly important for metastable helium atoms (2^3S), with an excitation energy of 19.8 eV, which is sufficient to ionize N_2, Ar, CO, etc. Associative ionization, in which the heavy particles bind to each other to form a molecular ion, can also occur.

Charge transfer reactions ($\mathbf{A}^+ + \mathbf{B} \rightarrow \mathbf{A} + \mathbf{B}^+$) can be resonant (typically if A = B) or non-resonant. The cross-section is much larger in the resonant case. Associative detachment ($\mathbf{A}^- + \mathbf{B}^+ \rightarrow (\mathbf{AB}^-)^* \rightarrow \mathbf{AB} + e$) is the most important electron detachment mechanism in non-equilibrium discharges. Collisions with excited particles ($\mathbf{A}^- + \mathbf{B}^* \rightarrow \mathbf{A} + \mathbf{B} + e$) can also lead to detachment if the excitation energy of collision partner B^* exceeds the electron affinity of particle A; the process is important in warm and thermal plasmas.

3.3.3 Equilibrium in Plasmas

The properties of plasmas can be described in terms of equilibrium statistical distributions. The Maxwell–Boltzmann distribution of kinetic energies was given by Eq. (3.4). The distribution of excited states can be described by a Boltzmann distribution:

$$n_j = n_0 \frac{g_j}{g_0} \exp\left[-\frac{(E_j - E_0)}{k_B T} \right] \tag{3.19}$$

where n_j and n_0 are the number densities of particles in the state j and the ground state, respectively, g_j and g_0 are the statistical weights of the two states, and E_j and E_0 are the energies of the two states.

Ionization equilibrium (for the reaction $\mathbf{A} \leftrightarrow \mathbf{A}^+ + e$) is described by the Saha equation:

$$\frac{n_e n_i}{n_a} = \frac{g_e g_i}{g_a} \left(\frac{m_a T}{h} \right)^{3/2} \exp\left(-\frac{E_{\text{ion}}}{k_B T} \right) \tag{3.20}$$

where subscripts e, i, and a refer to electrons, ions, and atoms, respectively, and h is Planck's constant. A similar expression can be used to describe dissociation equilibrium.

Plasmas in which all species follow the Maxwell–Boltzmann distribution (3.4) for translational energy distribution, the Boltzmann distribution (3.19) for all

excited states, the Saha Eq. (3.20) for ionization equilibrium, and chemical equilibrium equations for all dissociation and other reactions, with the same temperature applying in each case, are said to be in LTE. Complete thermodynamic equilibrium (CTE), which also requires the spectral density to follow a Planck distribution, is never realized in laboratory plasmas. However, most regions of thermal plasmas can usually be described by LTE because of the high collision rate at atmospheric pressure. However, the large gradients that occur in the edge regions and close to the electrodes in thermal plasmas can lead to departures from LTE. Such regions can often be described as two-temperature plasmas, with $T_e > T_h$. In this case, electrons and heavy particles follow separate Maxwell–Boltzmann distributions, and the Boltzmann distributions of excited electronic and vibrational states are described by T_e. The equilibrium of chemical reactions driven by electrons is largely determined by the electron temperature; as a consequence, the Saha equation is modified [8].

As discussed in Section 3.1.2, equilibration between translational energies of electrons and heavy particles takes tens to hundreds of nanoseconds, and shorter-lived discharges do not reach LTE. In most cases, separate Maxwell–Boltzmann distributions can still be applied to electron and heavy-particle translational energies, and the rotational excitation temperature $T_{\mathrm{rot}} \approx T_h$. However, since vibrational excitation can be much faster than VT relaxation, the vibrational temperature T_{vib} is often higher than T_h. Further, higher vibrational states can have higher densities than given by the Boltzmann distribution. This accelerates the rate of chemical reactions in which the vibrational states take part in accordance with Eq. (3.17).

The differences in T_e, T_h, and T_{vib} that occur in non-equilibrium plasmas lead to departures from chemical equilibrium. Departures can also occur when rates of particle transport (diffusion and convective flow) exceed rates of chemical reactions. For example, recombination reactions between atoms require three-body interactions to conserve momentum and kinetic energy and are therefore relatively slow; even in plasmas in thermal equilibrium, the rapid diffusion driven by steep temperature gradients can lead to more atoms being present at low temperatures than predicted by chemical equilibrium [17].

Departures from non-equilibrium chemistry facilitate many plasma applications. Nevertheless, in gas production applications, chemical equilibrium considerations often determine the optimum plasma type for a given reaction, with higher temperatures being favored for reactions with negative enthalpy ΔH and positive entropy ΔS, since the Gibbs free energy $\Delta G = \Delta H - T\Delta S$ decreases with increasing temperature.

3.4 Plasma Technology

Over the past 150 years, plasmas have been increasingly used for a huge range of applications including lighting, welding, cutting, deposition, water disinfection, mineral processing, semiconductor etching, and gas cleaning. The applications take advantage of many different plasma capabilities, including providing high temperatures and high fluxes of energy, reactive species, energetic ions, and radiation, which promote physical changes and chemical reactions that are inaccessible in the non-ionized gas phase. Most of these capabilities are only accessible with particular types of plasma. Accordingly, a wide range of plasma reactors has been developed to produce plasmas with the required properties. Reactor design is the subject of Chapter 4. This section considers the range of plasma types and properties that are used in applications and the principles underlying the production of the corresponding plasmas.

The plasma types of industrial interest in Figure 3.1 are labeled as glow discharges, DBDs, and warm plasmas (examples of non-equilibrium atmospheric-pressure discharges), and arcs (an example of thermal plasmas). The range of electron temperatures, approximately 1–10 eV, is relatively narrow, while the range of electron densities, from 10^{16} to 10^{25} m^{-3}, is much greater. The latter reflects wide ranges of both pressure and fractional ionization n_e/n. Pressure is determined by the filling pressure of the vessel containing the plasma (or the surrounding atmosphere if there is no vessel) and the energy supplied to the plasma. The fractional ionization depends on these factors, as well as the lifetime and dimensions of the plasma.

Energy can be supplied by different methods. The great majority of plasmas of industrial interest are generated by electric fields with frequencies ranging from DC to microwave. DC plasmas are generated between two electrodes, with the current being carried by electrons and ions. AC plasmas are excited by AC electric fields in the range from 50 Hz to around 100 kHz; the frequency is low enough for the ions to follow the oscillation of the field, so both electrons and ions contribute to the current. In both DC and AC plasmas, Joule heating dominates. For RF plasmas (in the MHz range), the excitation frequency exceeds the ion plasma frequency for the lower ion densities that occur at the low pressures typically used for such plasmas (see Section 3.1.2), so the ions remain almost at rest. Further, the displacement current rather than conduction carries the current. As well as Joule heating of the bulk plasma, stochastic heating (in which the electrons from the bulk plasma collide with the sheath regions) is significant. Finally, in microwave plasmas (in the GHz range), while the electrons can still (just) follow the field, the electromagnetic wave cannot fully penetrate the plasma because the skin depth of the wave is smaller than the plasma radius.

3.4.1 Low-Pressure Plasma Applications

Low-pressure plasmas, which are typically glow discharges, are used for the etching of metals and semiconductors, deposition and growth of thin film coatings, functionalization of surfaces, and generation of light. Typical pressures are in the range of 0.1–100 Pa (10^{-6}–10^{-3} bar), and the value of pd is usually less than $pd_{\min}$ (see Eq. (3.15)).

Plasma etching typically uses an RF discharge; coupling to the plasma can be capacitive, inductive, or through excitation of a plasma wave. The aim of the process is to transfer patterns, usually defined by lithography, into a thin film, meeting specifications for etching rate, material selectivity, feature size, and aspect ratio. A critical advantage of plasma etching over liquid- or vapor-phase techniques is that plasmas can etch a substrate anisotropically. Anisotropy is critical in integrated circuit manufacturing, where the spacing between features is now in the 5–10 nm range, and is achieved by the production of energetic ions directed toward the substrate. The ion energy distribution function depends on sheath potential and width and the ion mean free path, mass, and transit time compared to the RF period $2\pi/\omega$ [9]. Large mean free paths require low pressure, for which the time between collisions is large (see Figure 3.2d); however, this also decreases the plasma density and etching rate. This is no longer a critical problem since modern etching equipment can control both plasma density and ion bombardment characteristics independently [18].

Plasma deposition is achieved using many techniques, which are based on chemical vapor deposition (CVD) or physical vapor deposition (PVD). CVD uses high temperatures to promote gas-phase chemical reactions that produce reactive species that are deposited on a substrate, while PVD uses physical means, such as heating or ion sputtering, to produce the gas-phase species from a target.

The application of a plasma to CVD and PVD has several advantages. The process can take place at a lower temperature, allowing heat-sensitive substrates to be used. Applying a bias voltage to the substrate can be used to accelerate ionized precursors; these energetic ions transfer energy to the film, changing the film's composition and structure. For example, the top layer of the film can be annealed, improving and stabilizing the film properties without the need for a separate post-annealing process [18].

Plasma-enhanced CVD (PECVD) typically uses an RF plasma. The plasma makes available a greater range of species, including radicals and molecular fragments, which are mainly produced by electron-impact dissociation of gas-phase species. Higher deposition rates (1–10 nm s^{-1} or more) can be achieved than by CVD [19]. A wide range of pressures is used, depending on the required film composition and properties. PECVD is used for the deposition of many materials, including hydrogenated amorphous silicon (a-Si:H), mono- and nanocrystalline

silicon (mc/nc-Si), hydrogenated silica (SiO_2:H) and silicon nitride (SiN_x:H), diamond-like carbon, TiN, and TiO_2, which are used, e.g. in solar cells, integrated circuits, and as wear-resistant and low-friction coatings.

Plasma-enhanced PVD methods include magnetron sputtering and cathodic arc deposition [20]. Magnetron sputtering is a plasma-enhanced PVD process in which permanent magnets are placed behind the target to produce a magnetic field that restricts electron motion, increasing the plasma density and, therefore, the flux of ions to the target. The plasma is produced using a DC discharge if the target is metallic or an RF discharge for an insulating target. HiPiMS (high-intensity impulse magnetron sputtering) is a recently developed process that uses a pulsed high-power plasma to increase the ionization of sputtered atoms and create high fluxes of depositing atoms.

Cathodic arcs use the action of short-lived DC arcs between the cathode (the material to be evaporated) and an anode to produce a high flux of ions. The ions are produced from "cathode spots," which are small transient molten regions, and are accelerated up to $\sim 10^5$ m s^{-1} by the strong local pressure gradient and electric field of the expanding plasma. Cathodic arcs can be operated at very low pressures, or a gas can be added to react with the ions. The ions can be steered by a magnetic field to eliminate macroparticles before deposition onto a substrate. Applications include the deposition of wear-resistant tool coatings such as TiN and TiAlN and diamond-like carbon [18].

Low-pressure lamps, such as the fluorescent lamps used for domestic and industrial lighting, are gradually being replaced by LED lamps. In most discharge lamps, an AC current between two electrodes at either end of a glass tube is used to produce a glow discharge in low-pressure argon, with a small amount of mercury vapor used to emit UV radiation at 254 nm. For visible lighting, a phosphor is deposited on the inside of the glass tube. For UV lighting, used for disinfection and ozone production, no phosphor is used, and the glass is replaced by quartz to ensure good transmission. RF inductive coupling is also used, particularly for more powerful lamps [21].

While, in principle, low-pressure plasmas could be used for ammonia and NO_x synthesis, the production rate would be strongly limited by the low gas density, so such a system would be unlikely to be of practical interest.

3.4.2 Non-equilibrium Atmospheric-Pressure Plasma Applications

Non-equilibrium atmospheric-pressure plasmas have been used for over a century for the production of ozone and for many decades for surface functionalization and electrostatic precipitation [22]. In the past 10–20 years, a much wider range of applications, such as gas cleaning and production, human medicine including disinfection, wound treatment and cancer treatment, food disinfection, and

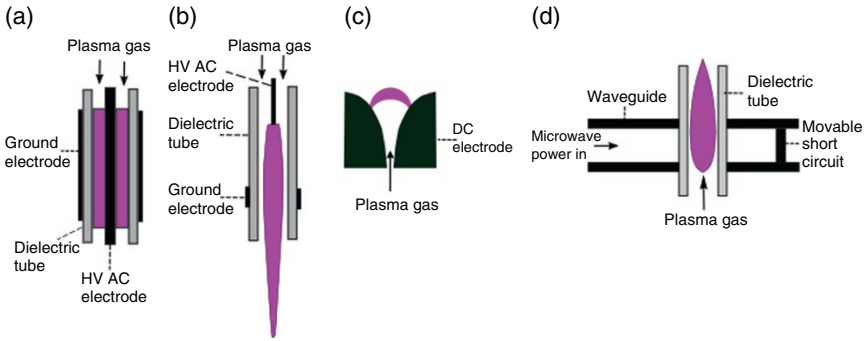

Figure 3.6 Schematics illustrating (a) cylindrical dielectric barrier discharge, (b) atmospheric-pressure plasma jet, (c) gliding arc discharge, and (d) microwave discharge.

promotion of seed germination and plant growth, have been developed and are, in some cases, in commercial use.

We can differentiate between non-equilibrium cold plasmas, where the gas temperature ranges from room temperature to several hundred kelvin, and non-equilibrium warm plasmas, where the gas temperature may be as high as a few thousand kelvin. In both cases, the electron temperature is at least 10,000 K.

Cold plasmas are generally glow discharges or corona discharges. An important consideration in generating a cold plasma is preventing the transition from a streamer to a spark or arc discharge, as noted in Section 3.2. Common methods are the imposition of one or more dielectric barriers between the electrodes (the DBD), shown schematically in Figure 3.6a, and limiting the discharge duration by using a nanosecond-pulsed power supply. In both cases, the discharge duration is typically less than 100 ns. The dielectric barrier is effective because charge builds up on the dielectric, reducing the electric field to below that required to sustain the discharge.

Using a high gas flow or a noble gas, for which vibrational excitation does not occur, also reduces the heating of the heavy particles and delays the transition to a spark. This approach has been applied to atmospheric-pressure plasma jets (see Figure 3.6b), in which gas is passed through a narrow ($\sim$1 mm radius) tube and ionized using a high-frequency AC voltage. In most cases, a dielectric barrier is used between the electrodes, but this is not always required. Microplasmas, in which an array of small ($\sim$100 μm or less) plasmas is produced, are stabilized using a ballast resistor to limit the current and therefore heating [23].

DBDs are particularly widely used. Many configurations have been developed [24]. Figure 3.6a shows a cylindrical DBD with the dielectric barrier adjacent to the ground electrode. The dielectric barrier can also be adjacent to the high-voltage

electrode, or two dielectric barriers can be used. Parallel flat-plate electrodes are an alternative to a cylindrical configuration. The discharge gap is in the range of 0.1–10 mm, and the voltage required is in the range of 1–100 kV, depending on the thickness of the discharge gap and the dielectric(s). Such DBDs are called "volume DBDs" because the discharge occurs in the gas gap volume. The plasma is usually in the form of large numbers of spatially localized microdischarges of radius about 100 μm, which are initiated shortly before the peak voltage is reached on each half cycle of the applied AC voltage. The microdischarges are initiated by a cathode-directed streamer, followed after a few nanoseconds by an anode-directed streamer, with a channel formed when the streamers reach the electrode and dielectric, spreading to broader surface discharges on the electrode and dielectric. In a 1 mm air discharge gap, the duration of the individual microdischarges is between 10 and 100 ns; the duration can be longer in argon [9]. Typical electron densities in the microdischarges are 10^{20} to 10^{21} m^{-3} [22]. The reduced electric field is large, usually 100 Td or more, leading to high electron energies (at least 10 eV), which couple to dissociation and ionization reactions rather than vibrational excitation (see Figure 3.5). As noted above, the microdischarges extinguish because the charge transferred to the dielectric barrier reduces the electric field across the gas gap.

It is possible, e.g. by lowering the pressure, using helium or helium-rich gases, or choosing particular electrode arrangements, to obtain diffuse non-filamentary discharges [22, 25]. Another option is surface DBDs, in which the electrodes are placed on either side of the dielectric, with the discharge appearing on the exposed dielectric surface next to the electrode that does not cover the whole dielectric surface.

Packed-bed DBDs are usually cylindrical, with the discharge region filled with beads of a dielectric material. Packed-bed DBDs combine both volume and surface discharges since microdischarges occur both along the surface of the beads and in the gaps between the beads. They are a widely used arrangement for plasma catalysis and plasma gas cleaning since they allow close contact between the plasma and the catalytic or reactive surface. Plasma catalysis is an intensively researched application of non-equilibrium atmospheric-pressure plasmas. The plasma provides energy to the reactants, allowing catalytic surface reactions to occur at lower gas temperatures and pressures than in thermal catalysis [26].

Atmospheric-pressure plasma jets are usually DBDs, as noted above. Different electrode arrangements are used, including the pin high-voltage electrode and ring ground electrode shown in Figure 3.6b. Such jets allow treatment of a surface by the non-equilibrium plasma, which can have a heavy-particle temperature close to ambient if the plasma gas is a noble gas. This suits the jet to the treatment of heat-sensitive surfaces, facilitating applications such as sterilization of foods and other materials, direct application to skin for wound healing, and treatment of

dermatological conditions [27]. Floating electrode DBDs are also used for such applications [28]. FE-DBDs usually have a flat plate high-voltage electrode covered by a dielectric, with the biological material serving as the ground electrode.

The interactions of atmospheric-pressure plasmas with liquids are critical in many applications. The discharge can occur within the liquid, above the liquid surface (possibly with the liquid serving as an electrode), in bubbles inside the liquid, and in a dispersed liquid (an aerosol) [29]. Applications such as wound and food treatment rely on the complex chemical reactions occurring at the boundary between the plasma and the biological material, particularly those involving reactive oxygen and nitrogen species. Discharges within the liquid can take the form of streamers or pulsed spark-type discharges. Bubble-type discharges can be formed by feeding gas through an electrode or through a separate gas diffuser. An important application of plasma discharges in liquids and bubbles is water treatment, with the degradation of many organic contaminants, including PFAS (per- and poly-fluoroalkyl substances), having been demonstrated [30].

Warm plasmas can be produced using sparks, microwave discharges, and gliding arc discharges. Spark discharges occur between two electrodes with a DC or AC voltage applied, but with the current limited to a few amperes. Gliding arc discharges use two electrodes whose separation increases with height, as shown in Figure 3.6c. A DC arc is struck at the bottom, where the separation is small, and convection moves the arc upward until it is too long to be supported by the power supply voltage, increasing the degree of non-equilibrium and eventually causing the arc to extinguish. Rotating gliding arc discharges apply swirl to the gas flow, allowing a larger proportion of the gas to pass through the discharge zone. Microwave discharges can be produced by many means; the most common arrangement at or near atmospheric pressure is for the plasma to be ignited in a dielectric tube inserted through a waveguide (Figure 3.6d). Microwave discharges are often operated somewhat below atmospheric pressure, which gives a broader plasma region.

Typical warm plasma electron densities at 1 bar are around 10^{18} to $10^{19}\,\mathrm{m}^{-3}$, electron temperatures are in the range of 1–2 eV, and heavy-particle temperatures are at least 1,000 K. Warm plasmas are characterized by high levels of vibrational excitation, which is facilitated by the relatively low E/N values, typically around 10 Td, as illustrated in Figure 3.5.

Both cold and warm atmospheric-pressure plasmas are widely used in the research and development of gas conversion processes. As discussed in Section 3.3.3, the choice is, to a significant extent, governed by the thermodynamics of the reaction. Processes such as ozone production from oxygen, ammonia production from nitrogen and hydrogen, and carbon dioxide methanation are exothermic and decrease entropy, so chemical equilibrium favors low temperatures, i.e. cold plasmas. Production of nitric oxide from nitrogen and oxygen,

carbon dioxide splitting, and dry reforming of methane are endothermic and maintain or increase enthalpy and are therefore favored by high temperatures, i.e. warm plasmas. The presence of a catalyst is important if selectivity is required (e.g. in carbon dioxide hydrogenation reactions) and can also assist in reducing energy barriers.

Results bear out these points. For example, extensive research on carbon dioxide splitting and dry reforming of methane has been carried out using dielectric barrier, gliding arc, and microwave discharges, with the best conversion and energy efficiencies obtained in the warm plasmas [31]. Similarly, warm plasmas outperform cold plasmas in nitric oxide production [32]. Commercial ozone production uses DBDs, with water cooling used to keep the temperature as low as possible [22]. Ammonia production has been shown to be favored by DBDs and the presence of a catalyst [15], as discussed in Section 3.5. Carbon dioxide methanation requires an appropriate catalyst and is again performed successfully in a DBD [33].

3.4.3 Thermal Plasma Applications

Thermal plasmas are those in which the electron temperature and heavy-particle temperature are approximately equal. Large regions of thermal plasmas are typically in LTE. As discussed in Section 3.3.3, this requires a high collision frequency, which in turn requires a pressure close to or above 1 bar (see Figure 3.2d). The level of ionization is high – at least 5% single ionization, and often 100% single ionization and significant double ionization. At atmospheric pressure, once full single ionization is reached, $n_e \approx 2 \times 10^{23}\ \mathrm{m}^{-3}$.

The typical mechanism of thermal plasma formation, discussed in Section 3.2, involves the initiation of a streamer discharge that spans the gap between two electrodes to form a spark discharge, with a power supply that can provide the current necessary to maintain the discharge. The high electron density leads to a relatively low resistance, so the voltage is generally low – corresponding to $E/n \sim 2\ \mathrm{kV\ m}^{-1}$ in the arc column plus about 10–30 V across the sheath regions. This is well below the electric field required to break down air (see Figure 3.4), so a thermal plasma is generally initiated by short-circuiting and then separating the electrodes or with an RF pulse to reduce the breakdown voltage. Thermal plasmas can also be produced by an inductively coupled RF field.

We can divide thermal plasmas into three main classes, based on their excitation mechanism and electrode configuration, as shown in Figure 3.7 [8, 34].

Transferred arcs are formed between two electrodes, one of which is the "workpiece" – the material being processed by the plasma. Transferred arcs are usually DC but can also be low-frequency AC. Transferred arcs can reach temperatures of 20,000 K or more and are characterized by high current densities (up to about $10^8\ \mathrm{A\ m}^{-2}$), which heat the plasma by Joule heating. The high temperature

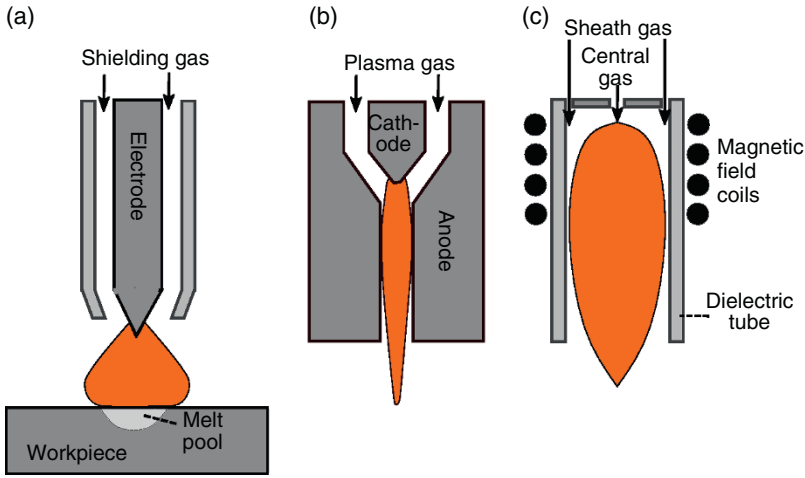

Figure 3.7 Schematics illustrating (a) transferred arc, (b) non-transferred arc, and (c) inductively coupled RF thermal plasma. *Source:* Ref. [34]/with permission of IOP Publishing.

leads to intense radiative emission. The high heat fluxes associated with the high temperatures and current densities allow metals and other materials to be melted; this is applied in arc welding, plasma cutting, plasma waste treatment, electric arc furnaces for metallurgical applications, and chemical applications. Arc currents for most such applications are in the range from 50 to 500 A but can be much higher in metallurgical applications. For such currents, the interaction between the current and the self-induced magnetic field leads to a strong magnetic pinch ($\boldsymbol{j} \times \boldsymbol{B}$) force, which increases the pressure and drives flow, with flow speeds reaching several hundred meters per second. The strong radiative emission is used in arc lamps, e.g. in car headlights and data and movie projectors. In such lamps, a short, low-current arc is initiated between two electrodes in gas at several bars; the gas flow speed is much lower and is driven by buoyancy rather than the magnetic pinch force.

Non-transferred arc plasmas are also formed between two electrodes, but in this case, the electrodes are within a "plasma torch," which produces a jet of plasma through an aperture in one of the electrodes. While the temperature within the torch can reach 25,000 K or more, the jet temperature is typically lower than 15,000 K at the aperture and cools rapidly in the atmosphere. The high temperature within the torch leads to rapid thermal expansion, and the plasma jet reaches high speeds, hundreds to thousands of meters per second, and is often supersonic (even though the speed of sound increases with temperature because of the decreased mass density). The most important application of non-transferred arcs

is plasma spraying, in which a ceramic powder is injected into the jet, which melts and accelerates the particles onto a substrate, forming a coating of thickness up to around 0.1 mm. Typical applications are thermal barrier coatings on jet engine turbine blades and wear-resistant coatings on paper rollers. Non-transferred plasmas are also used for plasma waste treatment and gasification, for gas heating (e.g. to simulate the heat fluxes that occur in space vehicle re-entry into the atmosphere), and for chemical production.

Inductively coupled RF plasmas are induced by a coil carrying RF current that is wound around a dielectric tube, with the plasma ignited inside the tube. The maximum temperature is significantly lower than in arc plasmas, typically around 12,000 K, and the temperature gradients are lower. Applications such as particle spheroidization and nanoparticle production take advantage of the relatively uniform plasma, which provides similar temperature histories for all precursors [8, 35]. In particle spheroidization, particles with sizes in the range of 10–100 μm are fed into the top of the plasma, where they melt and form spheres. A typical application is the production of metal powders for additive manufacturing. Nanoparticle production uses a solid, liquid, or gaseous precursor that is fed into the top of the plasma; a rapid quench of the flow at the bottom of the plasma leads to nucleation of particles in the 10–100 nm size range. Inductively coupled RF plasmas are also a critical component of analytical chemistry methods such as ICP-MS and ICP-OES (inductively coupled plasma – mass spectroscopy and optical emission spectroscopy); the chemical to be tested is dissolved in a liquid and injected into the plasma, where it is vaporized, and the elemental chemical composition is measured by MS, OES, or another analytical technique [36].

Thermal plasmas have been and continue to be successfully applied to large-scale chemical production [8, 16]. The Birkeland–Eyde process that was developed for NO_x production will be discussed in Section 3.5. The Hüls process, initially developed in the 1940s, continues to be used for the production of acetylene from methane and hydrogen, with the methane introduced downstream of hydrogen in a non-transferred arc [8, 37]. The Tioxide process used a non-transferred arc to produce pigment-grade titanium dioxide from titanium tetrachloride vapor and oxygen [8]. Thermal plasmas are now being used to pyrolyze methane, producing carbon black and hydrogen. The largest such facility, run by Monolith in Ohio, USA, uses a transferred arc process [38]. The hydrogen is used as the input for producing ammonia by the Haber-Bosch process, while the carbon black is sold to the tire industry. The process uses less than 20% of the energy required to produce hydrogen by electrolysis of water. Non-transferred arcs are also being used for methane pyrolysis.

3.5 Role of Plasma in Ammonia and NO_x Synthesis

The oxidation of nitrogen in a plasma to form NO_x was first reported by Lord Rayleigh in 1897 [39]. He used a ~1 kW transferred arc plasma between two platinum electrodes in a 50 L glass vessel supplied with a mixture of 45% air and 55% oxygen. The gas produced was passed through an alkali solution to produce about 50 g of nitric acid per hour.

The production of NO_x was one of the earliest industrial implementations of plasmas. The Birkeland–Eyde process [40, 41], developed in the early 1900s, used a thermal arc plasma between water-cooled copper electrodes to produce NO from air, with subsequent oxidation to NO_2 in a separate oxidation chamber, and reaction with water to form a nitric acid solution. The first plant was used in potassium nitrate manufacture in Notodden, Norway, with three 0.5 MW arc furnaces. A commercial plant was established in Niagara Falls, Canada, using hydroelectric power [42]. The power supplied increased from 2 kW in 1903 to 239 kW in 1928, with up to 38 kt of nitrogen fixed each year. The process produced 1–2 mol% NO and consumed 2.4–3.1 MJ mol^{-1} N.

The invention of the Haber–Bosch process for ammonia production, whose energy requirements are much lower, eventually led to the demise of the Birkeland–Eyde process. Only recently, with the growing importance of renewable energy sources and carbon emission reduction, have electrically based processes such as those using plasmas become prominent again.

The production of NO_x and NH_3 provides illustrative examples of the diverse chemical reactions that can occur in a plasma. Production of NO is an endothermic reaction:

$$N_2 + O_2 \rightarrow 2NO \quad \Delta H_0 = 90.3\ \text{kJ mol NO}^{-1} = 0.936\ \text{eV molecule NO}^{-1} \tag{3.21}$$

However, the standard entropy is positive (12.4 J K^{-1} mol NO^{-1}), so the Gibbs free energy becomes negative as temperature increases. For a mixture of 80% nitrogen and 20% oxygen, the maximum NO production in chemical equilibrium is about 2% and occurs around 3,500 K. As the temperature increases further, the NO dissociates. The theoretical minimum energy requirement in a thermal plasma, based on the energy required to break the N_2 triple bond (945 kJ mol^{-1} = 9.79 eV) and the O_2 double bond (498 kJ mol^{-1} = 5.16 eV), is 0.72 MJ mol NO^{-1}.

The reaction to produce NO proceeds via the Zeldovich mechanism:

$$\begin{aligned} N_2 + O &\rightarrow NO + N \\ O_2 + N &\rightarrow NO + O \end{aligned} \tag{3.22}$$

The first of these reactions has an energy barrier of about 8 eV, which is reduced to about 3 eV for vibrationally excited nitrogen. This gives a theoretical minimum energy requirement of just 0.2 MJ mol NO^{-1} in the case of optimum vibrational excitation [42]. Accordingly, warm plasmas such as spark, microwave, and gliding arc discharges, in which energy is coupled to vibrational modes, offer the best energy efficiencies, with approximately 2 MJ mol NO^{-1} being obtained. This is still well above the theoretical maximum, partly because of VT coupling taking energy away for vibrational modes. Another problem is the reverse reaction, which is favored by chemical equilibrium as the plasma cools; rapid quenching is therefore beneficial.

In contrast to NO production, NH_3 production is exothermic at room temperature:

$$N_2 + 3H_2 \rightarrow 2NH_3 \quad \Delta H^0 = -45.9 \text{ kJ mol } {NH_3}^{-1} = -0.476 \text{ eV molecule } {NH_3}^{-1} \tag{3.23}$$

and the standard entropy is negative. Therefore, chemical equilibrium favors low temperatures. However, significant energy is required to overcome the energy barrier of the reaction. As discussed in Chapter 1, a catalyst is used to reduce the energy barrier; however, activation of the catalyst typically requires temperatures of around 500 °C, at which the equilibrium favors the reactants. The Haber–Bosch process used high pressures (over 100 bar) to shift the equilibrium toward the products and obtain reasonable NH_3 yields.

Plasmas can overcome these restrictions because the significant energy coupled to electrons allows the formation of N and H radicals, which can react with each other and N_2 and H_2 to form ammonia in the gas phase. Chemical equilibrium favors low-temperature plasma such as DBDs. Using such plasmas, ammonia can be formed at a gas temperature of 300 K and atmospheric pressure. However, the significant energy required to dissociate N and H means the energy efficiency is low; also, the NH_3 concentrations produced have been low. Consequently, researchers have focused on combining plasmas and catalysis. In this case, the lower energy pathways, such as vibrational excitation of N_2 in the plasma followed by dissociative adsorption on the catalyst, may be possible. Single-pass NH_3 yields of over 5% have been achieved, but while the energy efficiencies are much higher in the presence of a catalyst, they remain uncompetitive [15].

These are just two examples of the approaches used to fix nitrogen using plasma-based and plasma-assisted processes. Subsequent chapters, including Chapters 5, 6, 9, 10, 11 and 12, will provide a much more detailed assessment of the different approaches and their relative benefits and drawbacks.

3.6 Conclusions

Plasma technology harnesses the diverse chemical, physical, and electrical phenomena offered by electrical discharges to etch semiconductors, deposit thin and thick films, melt and process metals and minerals, treat surfaces, emit radiation, drive chemical reactions, and contribute to many other processes. Such applications are relied upon in industries including materials, metal, semiconductor, mineral and chemical processing, automotive and aerospace manufacturing, information technology, energy supply, environmental protection and remediation, and biomedical and are hence indispensable to the modern economy.

In this chapter, we have considered many of these applications from the perspective of the underlying plasma properties and processes. The huge range of electron densities and electron and heavy-particle temperatures that occur in different types of naturally occurring and technological plasmas can be classified according to Debye length, plasma frequencies, mean free paths and collision times, and other properties. These properties are helpful in understanding the different electrical breakdown processes and the wide variety of chemical reactions and physical phenomena that are taken advantage of in plasma applications. These chemical and physical phenomena, in turn, inform the choice of design parameters, including power supply frequency, voltage and current, background pressure, reactor geometry, and process gas composition and flow rate, that allow the underlying chemistry and physics to be tailored to a particular plasma application.

The renewed effort to electrify the chemical industry, motivated by the need to reduce carbon emissions, has highlighted the potential of plasmas for nitrogen fixation. The usefulness of plasmas driving the required reactions has been known for well over a century, and plasma technology was implemented for industrial NO_x production for over 25 years in the early 1900s. The many advances in the understanding of plasma processes and their applications, some of which we have considered in this chapter, form the basis for the renewed effort to apply plasmas for this important goal, as will be seen in the remainder of this book.

Nomenclature

A, B	constants [−]
$\boldsymbol{B}$	magnetic field strength [T]
D_{ion}	ionization length [m]
e	electronic charge [C]
E	electric field strength [V m^{-1}]
E_a	activation energy [J]

E_{af} activation energy of forward reaction [J]
E_{ar} activation energy of reverse reaction [J]
E_{ion} ionization energy [J]
$E_{\text{kin } j}$ kinetic energy of species j [J]
E_m excitation energy of metastable atom [J]
g_a statistical weight of atoms [−]
g_e statistical weight of electrons [−]
g_i statistical weight of ions [−]
g_j statistical weight of state j [−]
g_0 statistical weight of ground state [−]
h Planck's constant [J s]
$\boldsymbol{j}$ current density [A m^{-2}]
k_B Boltzmann's constant [J K^{-1}]
k_R reaction rate coefficient [m^3 mol^{-1} s^{-1}]
k_{R0} pre-exponential term for ground-state molecule in k_R [m^3 mol^{-1} s^{-1}]
l_e electron mean free path [m]
m_j mass of species j [kg]
n total number density [m^{-3}]
n_a number density of atoms [m^{-3}]
n_0 number density of particles in ground state [m^{-3}]
n_e electron density [m^{-3}]
n_j number density of particles in state j [m^{-3}]
n_0 number density of particles in ground state [m^{-3}]
Q_{ea} momentum transfer cross-section for electron-atom collisions [m^2]
P pressure [Pa]
T_e electron temperature [eV or K]
T_h heavy-particle temperature [K]
T_{vib} vibrational temperature [K]
V_b breakdown voltage [V]
v_d electron drift velocity [m s^{-1}]
Z_j charge number of species j
$\boldsymbol{v}_j$ velocity of species j [m s^{-1}]
v_j average velocity of species j [m s^{-1}]
v_{de} mean electron drift velocity [m s^{-1}]
τ_e mean time between electron collisions [s]
α ionization coefficient (first Townsend coefficient) [m^{-1}]
α_{FM} efficiency of excitation energy in overcoming reaction barrier [−]
β recombination coefficient (second Townsend coefficient) [m^{-1}]
Υ secondary ionization coefficient (third Townsend coefficient) [m^{-1}]
ΔH^0 standard reaction enthalpy [J]

η recombination coefficient [m^{-1}]
ε_0 permittivity of free space [$F\,m^{-1}$]
λ_D Debye length [m]
ω angular frequency of applied voltage [$rad\,s^{-1}$]
ω_{pj} plasma frequency of species j [$rad\,s^{-1}$]

References

1 Langmuir, I. (1928). Oscillations in ionized gases. *Proc. Natl. Acad. Sci.* 14 (8): 627–637. https://doi.org/10.1073/pnas.14.8.627.
2 Howatson, A.M. (1965). *An Introduction to Gas Discharges*. Oxford: Pergamon Press.
3 Von Keudell, A. and Schulz-von der Gathen, V. (2017). Foundations of low-temperature plasma physics—an introduction. *Plasma Sources Sci. Technol.* 26 (11): 113001. https://doi.org/10.1088/1361-6595/aa8d4c.
4 Devoto, R.S. (1973). Transport coefficients of ionized argon. *Phys. Fluids* 16 (5): 616–623. https://doi.org/10.1063/1.1694396.
5 Lelevkin, V.M., Ortobaev, D.K., and Schram, D.C. (1992). *Physics of Non-equilibrium Plasmas*. Amsterdam: North-Holland Publishing Company.
6 Itikawa, Y. (1974). Momentum-transfer cross sections for electron collisions with atoms and molecules. *At. Data Nucl. Data Tables* 14 (1): 1–10. https://doi.org/10.1016/S0092-640X(74)80026-4.
7 Itikawa, Y. (1978). Momentum-transfer cross sections for electron collisions with atoms and molecules. Revision and supplement, 1977. *At. Data Nucl. Data Tables* 21 (1): 69–75. https://doi.org/10.1016/0092-640X(78)90004-9.
8 Boulos, M.I., Fauchais, P.L., and Pfender, E. (2023). *Handbook of Thermal Plasmas*. Cham: Springer Nature https://doi.org/10.1007/978-3-030-84936-8.
9 Bruggeman, P.J., Iza, F., and Brandenburg, R. (2017). Foundations of atmospheric pressure nonequilibrium plasmas. *Plasma Sources Sci. Technol.* 26 (12): 123002. https://doi.org/10.1088/1361-6595/aa97af.
10 Pancheshnyi, S. (2005). Role of electronegative gas admixtures in streamer start, propagation and branching phenomena. *Plasma Sources Sci. Technol.* 14 (4): 645–653. https://doi.org/10.1088/0963-0252/14/4/002.
11 Raizer, Y.P. (1997). *Gas Discharge Physics*, 2e. Berlin: Springer.
12 Montijn, C. and Ebert, U. (2006). Diffusion correction to the Raether–Meek criterion for the avalanche-to-streamer transition. *J. Phys. D. Appl. Phys.* 39: 2979–2992. https://doi.org/10.1088/0022-3727/39/14/017.

13 Lowke, J.J. (1992). Theory of electrical breakdown in air-the role of metastable oxygen molecules. *J. Phys. D. Appl. Phys.* 25 (2): 202–210. https://doi.org/10.1088/0022-3727/25/2/012.

14 Naidis, G.V. (2005). Conditions for inception of positive corona discharges in air. *J. Phys. D. Appl. Phys.* 38 (13): 2211–2214. https://doi.org/10.1088/0022-3727/38/13/020.

15 Rouwenhorst, K.H.R., Engelmann, Y., Veer, K.v.'t. et al. (2020). Plasma-driven catalysis: green ammonia synthesis with intermittent electricity. *Green Chem.* 22 (19): 6258–6287. https://doi.org/10.1039/D0GC02058C.

16 Fridman, A. (1998). *Plasma Chemistry*. Cambridge: Cambridge University Press.

17 Snyder, S.C., Murphy, A.B., Hofeldt, D.L., and Reynolds, L.D. (1995). Diffusion of atomic hydrogen in an atmospheric-pressure free-burning arc discharge. *Phys. Rev. E* 52 (3): 2999–3009. https://doi.org/10.1103/PhysRevE.52.2999.

18 Oehrlein, G.S. and Hamaguchi, S. (2018). Foundations of low-temperature plasma enhanced materials synthesis and etching. *Plasma Sources Sci. Technol.* 27 (2): 023001. https://doi.org/10.1088/1361-6595/aaa86c.

19 Martinu, L. and Poitras, D. (2000). Plasma deposition of optical films and coatings: a review. *J. Vac. Sci. Technol. A* 18 (6): 2619–2645. https://doi.org/10.1116/1.1314395.

20 Gudmundsson, J.T., Anders, A., and von Keudell, A. (2022). Foundations of physical vapor deposition with plasma assistance. *Plasma Sources Sci. Technol.* 31 (8): 083001. https://doi.org/10.1088/1361-6595/ac7f53.

21 Zissis, G. and Kitsinelis, S. (2009). State of art on the science and technology of electrical light sources: from the past to the future. *J. Phys. D. Appl. Phys.* 42 (17): 173001. https://doi.org/10.1088/0022-3727/42/17/173001.

22 Kogelschatz, U. (2003). Dielectric-barrier discharges: their history, discharge physics, and industrial applications. *Plasma Chem. Plasma Process.* 23 (1): 1–46. https://doi.org/10.1023/A:1022470901385.

23 Schoenbach, K.H. and Becker, K. (2016). 20 years of microplasma research: a status report. *Eur. Phys. J. D - At. Mol. Opt. Phys.* 70: 29. https://doi.org/10.1140/epjd/e2015-60618-1.

24 Pietsch, G.J. and Gibalov, V.I. (2012). Dynamics of dielectric barrier discharges in different arrangements. *Plasma Sources Sci. Technol.* 21 (2): 024010. https://doi.org/10.1088/0963-0252/21/2/024010.

25 Massines, F., Gherardi, N., and Naudé, N.S. (2009). Recent advances in the understanding of homogeneous dielectric barrier discharges. *Eur. Phys. J. Appl. Phys.* 47 (2): 22805. https://doi.org/10.1051/epjap/2009064.

26 Bogaerts, A., Neyts, E.C., Guaitella, O., and Murphy, A.B. (2022). Foundations of plasma catalysis for environmental applications. *Plasma Sources Sci. Technol.* 31 (5): 053002. https://doi.org/10.1088/1361-6595/ac5f8e.

27 Weltmann, K.-D., Kolb, J.F., Holub, M. et al. (2018). The future for plasma science and technology. *Plasma Process. Polym.* 16 (1): 1800118. https://doi.org/10.1002/ppap.201800118.

28 Fridman, G., Peddinghaus, M., Balasubramanian, M. et al. (2006). Blood coagulation and living tissue sterilization by floating-electrode dielectric barrier discharge in air. *Plasma Chem. Plasma Process.* 26 (4): 425–442. https://doi.org/10.1007/s11090-006-9024-4.

29 Bruggeman, P.J., Kushner, M.J., Locke, B.R. et al. (2016). Plasma–liquid interactions: a review and roadmap. *Plasma Sources Sci. Technol.* 25 (5): 053002. https://doi.org/10.1088/0963-0252/25/5/053002.

30 Blotevogel, J., Thagard, S.M., and Mahendra, S. (2023). Scaling up water treatment technologies for PFAS destruction: current status and potential for fit-for-purpose application. *Curr. Opin. Chem. Eng.* 41: 100944. https://doi.org/10.1016/j.coche.2023.100944.

31 Snoeckx, R. and Bogaerts, A. (2017). Plasma technology – a novel solution for CO_2 conversion? *Chem. Soc. Rev.* 46 (19): 5805–5863. https://doi.org/10.1039/C6CS00066E.

32 Abdelaziz, A.A., Komuro, A.T., Schiorlin, Y.M. et al. (2024). Atmospheric-pressure plasmas for NO_x production: short review on current status. *Curr. Opin. Green Sust. Chem.* 50: 100977. https://doi.org/10.1016/j.cogsc.2024.100977.

33 Ullah, S., Gao, Y., Dou, L. et al. (2023). Recent trends in plasma-assisted CO_2 methanation: a critical review of recent studies. *Plasma Chem. Plasma Process.* 2023 (6): 1335–1383. https://doi.org/10.1007/s11090-023-10417-9.

34 Murphy, A.B. and Uhrlandt, D. (2018). Foundations of high-pressure thermal plasmas. *Plasma Sources Sci. Technol.* 27 (6): 063001. https://doi.org/10.1088/1361-6595/aabdce.

35 Boulos, M.I. (2016). The role of transport phenomena and modeling in the development of thermal plasma technology. *Plasma Chem. Plasma Process.* 36 (1): 3–28. https://doi.org/10.1007/s11090-015-9660-7.

36 Broekaert, J.A.C. (2005). *Analytical Atomic Spectrometry with Flames and Plasmas*. Weinheim: Wiley.

37 Gladisch, H. (1962). How Huels makes acetylene by DC arc. *Hydrocarbon Process. Petrol. Refiner* 41: 159–164.

38 Dames, E., Rohani, V., and Fulcheri, L. (2023). Plasma Chemistry and Plasma Reactors for Turquoise Hydrogen and Carbon Nanomaterials Production. In: *Turquoise Hydrogen: An Effective Pathway to Decarbonization and Value Added Carbon Materials* (ed. M. Pelucchi and M. Maestri), 253–317. Cambridge, MA: Elsevier https://doi.org/10.1016/bs.ache.2023.05.001.

39 Rayleigh, L. (1897). Observations on the oxidation of nitrogen gas. *J. Chem. Soc. Trans.* 71: 181–186. https://doi.org/10.1039/CT8977100181.

40 Birkeland, K. (1906). On the oxidation of atmospheric nitrogen in electric arcs. *Trans. Faraday Soc.* 2 (2): 98–116. https://doi.org/10.1039/TF9060200098.

41 Eyde, S. (1912). Oxidation of atmospheric nitrogen and development of resulting industries in Norway. *J. Ind. Eng. Chem.* 4 (10): 771–774. https://doi.org/10.1021/ie50046a025.

42 Rouwenhorst, K.H.R., Jardali, F., Bogaerts, A., and Lefferts, L. (2021). From the Birkeland–Eyde process towards energy-efficient plasma-based NO_X synthesis: a techno-economic analysis. *Energy Environ. Sci.* 14 (5): 2520–2534. https://doi.org/10.1039/d0ee03763j.